# The ATP-Binding Site of $Ca^{2+}$-ATPase Revealed by Electron Image Analysis

Koji Yonekura,*# David L. Stokes,§ Hiroyuki Sasabe,¶ and Chikashi Toyoshima*
*Institute of Molecular and Cellular Biosciences, the University of Tokyo, Bunkyo-ku, Tokyo 113, Japan; #Department of Biological Sciences, Tokyo Institute of Technology, Nagatsuta, Yokohama 226, Japan; §Skirball Institute of Biomolecular Medicine, New York University Medical Center, New York, New York 10016 USA; and ¶Frontier Research Program, RIKEN, Wako, Saitama 351-01, Japan

ABSTRACT The location of the ATP-binding site of a P-type ion pump, $Ca^{2+}$-ATPase from rabbit sarcoplasmic reticulum, was examined by cryoelectron microscopy. A nonhydrolyzable analog of ATP, $\beta,\gamma$-bidentate chromium (III) complex of ATP (CrATP), was used to stabilize the enzyme in the $Ca^{2+}$-occluded state. Tubular crystals were then induced by vanadate in the presence of EGTA, keeping CrATP bound to the enzyme. The three-dimensional structures of the crystals were determined at 14 Å resolution by cryoelectron microscopy and helical image analysis. Statistical comparison of the structures with and without CrATP showed clear and significant differences at the groove proposed previously as the ATP-binding pocket.

## INTRODUCTION

Sarcoplasmic reticulum (SR) $Ca^{2+}$-ATPase is an integral membrane protein of 110 kDa that pumps $Ca^{2+}$ into SR against a large concentration gradient during relaxation of muscle cells. To do so, it uses the chemical energy of ATP and transports two $Ca^{2+}$ per ATP hydrolysis. $Ca^{2+}$-ATPase is one of the members of the large P-type ion pump family, which includes $Na^+/K^+$-ATPase, gastric $H^+/K^+$-ATPase, and yeast $H^+$-ATPase, among others (for a recent review see Møller et al., 1996). These pumps share considerable sequence homologies, similar reaction cycles, and common domain structures. The proposed structural model for $Ca^{2+}$-ATPase consists of two main cytoplasmic domains connected by a narrow stalk to 10 transmembrane helices (M1–M10) (MacLennan et al., 1985; Brandl et al., 1986; Taylor and Green, 1989). Mutational analyses have revealed that the critical residues for $Ca^{2+}$ binding are located at the middle of putative transmembrane helices (Clarke et al., 1989; Chen et al., 1996) and that those for ATP hydrolysis are in the larger cytoplasmic domain between M4 and M5 (Maruyama et al., 1989; Clarke et al., 1990a; Vilsen et al., 1991). A number of chemical labels have been also used to locate the residues involved in the ATP binding (for a review see Bigelow and Inesi, 1992). The domain for ATP binding has been suggested to fold like nucleotide-binding domains of certain kinases (Taylor and Green, 1989), in which two subdomains connected by a hinge form a nucleotide-binding pocket. The smaller cytoplasmic domain between M2 and M3 presumably consists of antiparallel $\beta$-sheets (MacLennan et al., 1985) and is responsible for coupling of ATP hydrolysis to ion transport (Andersen et al., 1989; Clarke et al., 1990b).

*Received for publication 23 October 1996 and in final form 10 December 1996.*

Address reprint requests to Dr. C. Toyoshiman, Institute of Molecular and Cellular Biosciences, University of Tokyo, Bunkyo-ku, Tokyo 113, Japan. Tel.: 81-3-5689-7227; Fax: 81-3-5689-7227; E-mail: ct@imcbns.iam.u-tokyo.ac.jp.



0006-3495/97/03/997/09 $2.00

However, direct three-dimensional information for $Ca^{2+}$-ATPase is very limited. The highest resolution three-dimensional structure so far obtained is only at ~14 Å resolution (Toyoshima et al., 1993a). The resolution of this structure, obtained by cryoelectron microscopy from tubular crystals formed in the absence of $Ca^{2+}$ and ATP, was obviously too low for unambiguous location of functional sites. Nevertheless, we proposed a groove in the cytoplasmic domain as a candidate for the ATP-binding site (Fig. 1), based on the results from affinity labeling (see Green and Stokes, 1992, for a review). If correct, this location implies that the structural effects of $Ca^{2+}$ binding are transferred more than 40 Å to the ATP-binding site. The hydrolysis of ATP and phosphorylation of the enzyme in turn alter the conformation of the $Ca^{2+}$-binding sites to release $Ca^{2+}$ into the lumen of SR. Therefore, knowledge of the precise position of the ATP-binding site is a critical step in characterizing the long-range interactions within the enzyme and, ultimately, in understanding the mechanism of active transport.

In this paper we used $\beta,\gamma$-bidentate chromium (III) complex of ATP (CrATP) to locate the ATP-binding site directly and to investigate structural changes induced by ATP binding. This nonhydrolyzable analog of ATP has been used to stabilize the enzyme in the $Ca^{2+}$-occluded state (Serpersu et al., 1982; Vilsen and Andersen, 1987). Although the tubular crystals can be formed retaining CrATP bound (Buhle et al., 1983; Stokes and Lacapere, 1994), no three-dimensional structures have been obtained so far. We describe here the three-dimensional structure of $Ca^{2+}$-ATPase with bound CrATP and the differences caused by the binding of CrATP.

## MATERIALS AND METHODS

### Preparation of sarcoplasmic reticulum, CrATP, and decavanadate

SR was prepared from the white muscle of rabbit legs by the method of Meissner et al. (1973). Protein concentrations were determined using bicinchoninic acid reagent (Pierce Chemical Co., Rockford, IL; Smith et

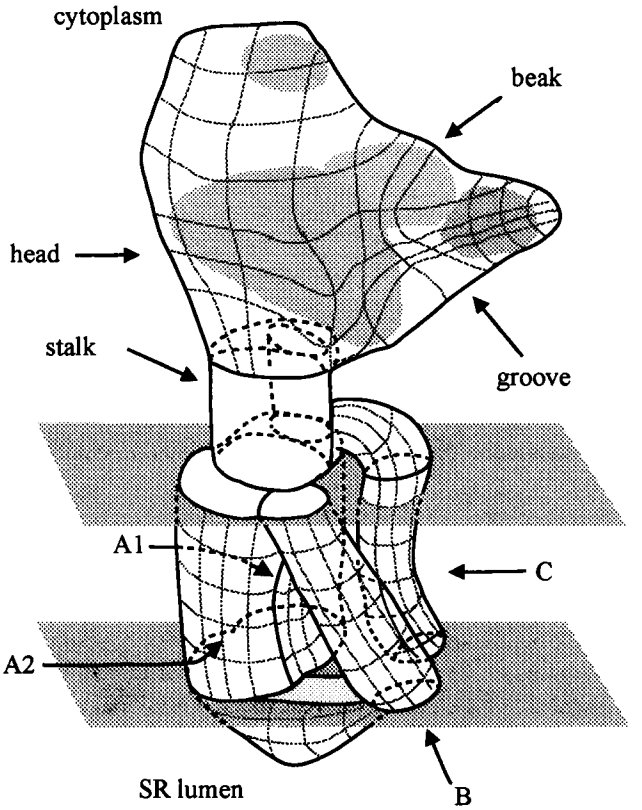


FIGURE 1 Cartoon of the structure of $Ca^{2+}$-ATPase in the absence of ATP and $Ca^{2+}$ as determined by cryoelectron microscopy. The surfaces of the bilayer are indicated by the two shadow planes. A large cytoplasmic domain, resembling the head of a bird, is linked to the membrane domain through a stalk region. The membrane domain consists of three segments, A, B, and C. A is further divided to subsegments, A1 and A2. The ATP-binding site is postulated to be at the "groove." The ion pathway in the membrane is proposed to be located at the interface between A1 and A2. Reproduced with permission from *Nature* (Toyoshima et al., 1993a).

al., 1985) after SR was completely dissolved in 1% (w/v) deoxycholate solution. Protein concentrations were also determined by the absorbance at 280 nm with an extinction coefficient of 1.05 ($ml \cdot mg^{-1} \cdot cm^{-1}$) (Thorley-Lawson and Green, 1973). These two procedures generally agreed within 10% (Chen et al., 1991). $\beta,\gamma$-Bidentate CrATP was prepared as described by Mariano and Cleland (1980) and Cleland (1982). Decavanadate stock solution was prepared by adjusting the pH of 50 mM $Na_3VO_4$ to 2.0 and incubating overnight at 4°C (Varga et al., 1985); the pH was neutralized immediately before adding to the crystallization solution.

## Tubular crystals of $Ca^{2+}$-ATPase with bound CrATP

SR (2 mg/ml) was reacted with CrATP in 100 mM KCl, 5 mM $MgCl_2$, 1 mM CrATP, 0.1 mM $CaCl_2$, and 10 mM imidazole, pH 7.4, at 25°C. After 4 h, an equal volume of the same buffer containing 10 mM vanadate and 1–2 mM EGTA instead of $Ca^{2+}$ was added and incubated at 4°C. Tubular crystals grew in 18–36 h (Buhle et al., 1983; Stokes and Lacapere, 1994).

## Assay of the effect of CrATP

Inhibition of $Ca^{2+}$-ATPase activity by CrATP was measured by a coupled ATPase assay (Warren et al., 1974). Five to ten microliters of the sample solution was added to 800 $\mu$l of the assay medium (150 mM KCl, 7.5 mM $MgCl_2$, 0.15 mM $CaCl_2$, 75 mM 3-(*N*-morpholino)propanesulfonic acid-KOH, pH 7.0, 0.5 mM phosphoenolpyruvate, 0.25 mM NADH, 7.1 IU pyruvate kinase, and 13.5 IU lactate dehydrogenase) and incubated for 5 min at 37°C. After an addition of 10 $\mu$l of 100 mM ATP, the decrease of NADH was monitored by the absorbance at 340 nm, which corresponded directly to the rate of ATP hydrolysis.

Occlusion of $^{45}Ca^{2+}$ was assayed by filtration (Chen et al., 1991; Vilsen and Andersen, 1992). After reaction with CrATP in the presence of 0.05–0.1 mM $^{45}Ca^{2+}$, 50–100 $\mu$l of the sample was filtered (0.45 $\mu$m, HAWP025; Millipore Co., Bedford, MA) and then washed with 30 ml of cold buffer. The filter that had retained the SR was completely dissolved in 3 ml of liquid scintillation cocktail (ASC II; Amersham International plc, Buckinghamshire, England), and the amount of $^{45}Ca^{2+}$ was determined by a liquid scintillation counter (LSC-5100; Aloka Co., Tokyo, Japan). This method allowed us to measure only the tightly bound $^{45}Ca^{2+}$ that did not dissociate within ~1 min.

## Electron microscopy

Four microliters of specimen solution were deposited on a carbon-coated holey grid and blotted with filter paper. The specimen was rapidly frozen by plunging into an ethane slush. A Gatan 626 cryoholder (Pleasanton, CA) was used for examination in a JEOL JEM-2000EX microscope (Tokyo, Japan) operated at 200 kV. Images were recorded on Kodak SO163 films at a nominal magnification of 40,000× using a low-dose kit. The objective lens current was monitored. The magnification was calibrated using negatively stained tropomyosin tactoids (Caspar et al., 1969) at various objective lens currents. Three images of tubes without CrATP were taken during the previous work (Toyoshima et al., 1993a) at a nominal magnification of 36,000×, using a Philips EM420T microscope (Mahwah, NJ) operated at 120 kV.

## Image analysis

Images of straight tubular crystals with the diameter of about 650 Å were selected and examined first by optical diffraction. Suitable images were digitized with 20-$\mu$m spot and step sizes with a flatbed microdensitometer (PDS1010 M; Orbital Science, Pomona, CA). The amounts of defocus were estimated from the Thon rings that arise from the images of carbon film or tubular crystals themselves (Tani et al., 1996). The amplitude contrast of 4.6% was assumed (Toyoshima et al., 1993b). Helical reconstruction was carried out essentially as described by Toyoshima and Unwin (1990). Weakly (6500–9500 Å) and strongly (about 20,000 Å) underfocused pairs of images taken of the same fields were used for a partial compensation of uneven contrast transfer function (CTF, Toyoshima and Unwin, 1990). This procedure was essential for comparison of individual images because good signal-to-noise ratio was required. The resolution was limited by the first CTF zero of the weakly defocused image.

Tubes belonging to the same helical family can usually be averaged in Fourier space by renumbering the layer lines, provided that the unit cell parameters are virtually identical (Toyoshima and Unwin, 1990). However, with tubes formed in the absence of CrATP, a helical family consisted of two groups of different diameters. In this case, because of large differences in unit cell parameters, averaging had to be done in real space instead of Fourier space. To do so, first, the tubes belonging to the same group of similar unit cell parameters were averaged separately in Fourier space. Next, the mean radial density distribution (MRDD) of each group was calculated by Fourier-Bessel synthesis of the equatorial layer line. Cross-correlation between MRDDs from the two groups was used to determine their relative magnifications. After magnification correction, three-dimensional maps of both groups were calculated independently. Then the density scaling was adjusted by linear regression. Finally, after one molecule was cut out from the map at the level enclosing 100% of expected volume, it was brought to the same position by applying rotational and translational adjustments. Then the density maps of one molecule were

averaged. For the tubes with bound CrATP, real space averaging was unnecessary because they all have similar unit cell parameters (Table 1).

To investigate the differences in the structure with and without CrATP, a difference map was calculated by subtracting the three-dimensional map of the enzyme without CrATP from that with CrATP. Furthermore, to examine the significance of the differences, Student's *t*-test was carried out (Milligan and Flicker, 1987) after density scaling of the individual images.

## RESULTS

### The effect of CrATP on $Ca^{2+}$-ATPase

The binding of CrATP, a nonhydrolyzable analog of ATP, was assessed by measuring the inhibition of the ATPase activity (Fig. 2, *filled circles*). After 4 h, ATPase activity was decreased to about 15% of the initial value. Because the $Ca^{2+}$-insensive ATPase activity was ~15%, the inhibition by CrATP was nearly complete. After the addition of vanadate to induce tubular crystals, the activity remained at the same level, consistent with the results of Stokes and Lacapere (1994). In contrast, with vanadate alone, the activity decreased to only ~60% of the initial value ( Fig. 2, *open circle after 20 h*). Hence, CrATP must be bound to $Ca^{2+}$-ATPase in the tubular crystals.

$^{45}Ca^{2+}$ was trapped within $Ca^{2+}$-ATPase when CrATP was bound to the enzyme (Fig. 2, *filled squares*). After 4 h, the amount of occluded $Ca^{2+}$ was about 1.6 mol/mol SR protein. Considering that the proportion of $Ca^{2+}$-ATPase in total membrane proteins in SR is ~80%, the value means that most of the enzyme had two $Ca^{2+}$s bound per molecule. Because the removal of free $Ca^{2+}$ was necessary for the formation of tubular crystals, EGTA as well as vanadate was added. As a consequence, when tubular crystals were formed, most of the occluded $Ca^{2+}$ was released into buffer (Fig. 2, *filled box after 20 h*).

### Image analysis of tubular crystals of $Ca^{2+}$-ATPase

A diffraction pattern of an image of a tubular crystal with bound CrATP is shown in Fig. 3 *b*. It consists of a series of layer lines symmetrical about the meridian, showing good preservation of helical symmetry. The qualities of the tubes with CrATP were indistinguishable from those without

**TABLE 1 Unit cell parameters for the tubes belonging to the (−25, 7) family**

| | Number of tubes | Radius (Å)* | *a* (Å)# | *b* (Å)# | γ (°)# |
|---|---|---|---|---|---|
| Narrower tubes without CrATP | 3 | 216.0 ± 0.8 | 59.0 ± 0.3 | 117.6 ± 2.6 | 65.4 ± 0.6 |
| Wider tubes without CrATP | 3 | 230.3 ± 4.0 | 58.0 ± 0.6 | 109.6 ± 3.4 | 74.6 ± 1.7 |
| Tubes with CrATP | 7 | 230.5 ± 2.9 | 58.4 ± 0.4 | 111.9 ± 2.6 | 73.5 ± 0.9 |

*The radii refer to the middle of the membrane as specified in Fig. 4.
#*a*, *b*, and γ are specified at the middle of the membrane; also see Fig. 5.

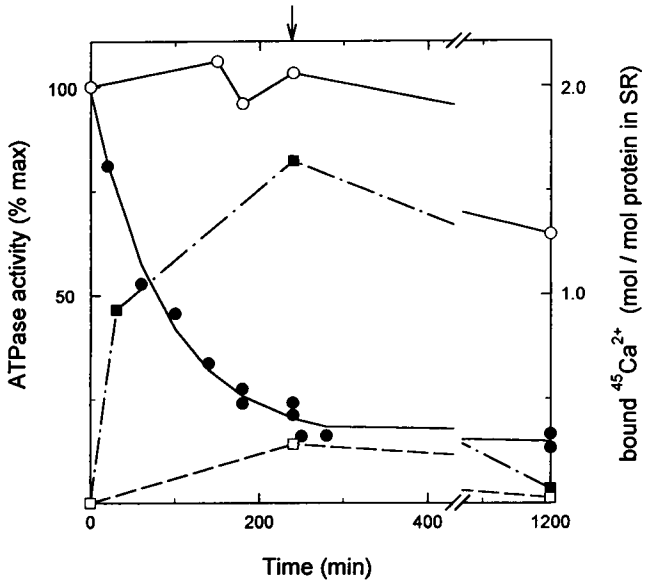


FIGURE 2 The effects of CrATP on $Ca^{2+}$-ATPase: ATPase activity (○, ●), and amounts of occluded $^{45}Ca^{2+}$ (□, ■). SR was incubated in the buffer containing CrATP (●, ■) or without it (○, □). The arrow at the top of this figure indicates the time when the crystallization buffer containing EGTA and vanadate was added.

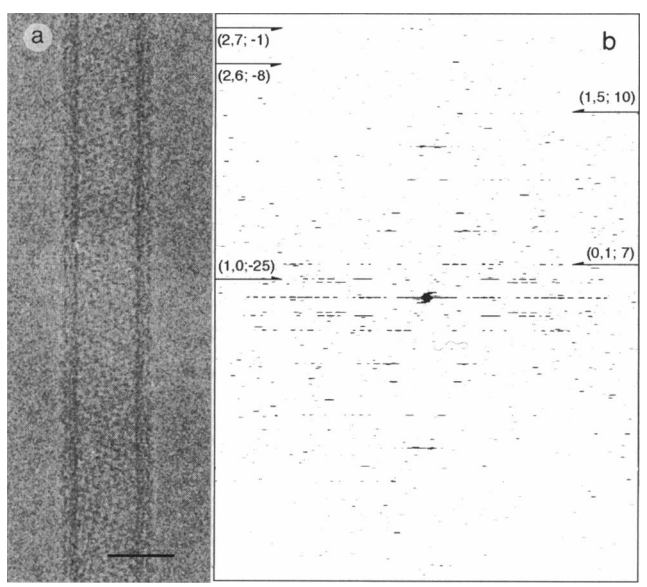


FIGURE 3 Electron micrograph of a tubular crystal of $Ca^{2+}$-ATPase in vitreous ice (*a*) and amplitudes of the Fourier transform (*b*) of an image of a region of the tube in *a*, taken at a smaller defocus than in *a*. The transform consists of a series of horizontal lines (layer lines), each corresponding to a set of helices. This tube belongs to the ($n_{10} = -25$, $n_{01} = 7$) family. (*h*, *k*) indices and start numbers on the associated surface lattice (see Toyoshima and Unwin, 1990) are indicated for some layer lines. The (2, 7; −1) layer line is located at the axial spacing of 1/15.4 $Å^{-1}$. The bar in *a* represents 500 Å

CrATP (cf. figure 1 *b* of Toyoshima et al., 1993a), as is demonstrated by the presence of a near-meridional layer line with an axial spacing of 1/15.4 $Å^{-1}$ (indexed as (2, 7; −1) in Fig. 3 *b*).

The symmetry of a tubular crystal can be characterized by two indices representing the start numbers of two principal helices ($n_{10}$ and $n_{01}$; see Toyoshima and Unwin, 1990). Similar to tubular crystals of other membrane proteins (e.g. Toyoshima and Unwin, 1990), those of $Ca^{2+}$-ATPase had a variety of helical symmetries slightly different from one another. We mainly collected the tubes belonging to the ($n_{10}$ = −25, $n_{01}$ = 7) or ($n_{10}$ = −26, $n_{01}$ = 7) families because they were found more frequently than the others and were narrow enough for helical reconstruction. The (−25, 7) family of tubes formed without CrATP consisted of two groups of different diameters (Fig. 4). The unit cell parameters (Table 1 and Fig. 5) were also different, and as a result, data from two groups were averaged in real space after Fourier space averaging of data within each group.

Table 2 summarizes the quality of the data sets. Because dimer ribbons were formed in the tubular crystals, twofold rotational symmetry normal to the helix axis was present and used as the measure of the quality of the images (Toyoshima and Unwin, 1988). Phase residuals for the twofold symmetry were similar for the tubes with and without CrATP. The twofold phase residuals for those belonging to the (−26, 7) family were 2.9° (with CrATP, 23 images) and 8.2° (without CrATP, 5 images).

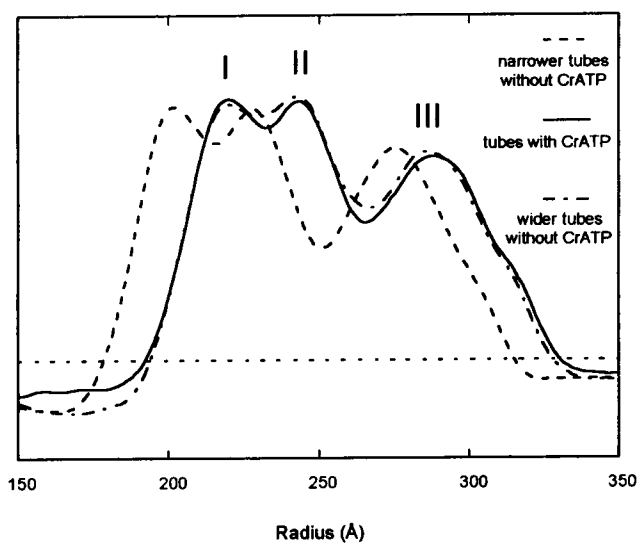


FIGURE 4 Mean radial density distribution ($g_{00}$) of the tubes belonging to the (−25, 7) family. The curves were obtained by Fourier-Bessel synthesis of the equatorial layer line after correcting for the effects of the CTF. The three peaks marked refer, respectively, to the densities at the inner (I) and the outer (II) leaflets of the lipid bilayer and the cytoplasmic domain (III). The minimum between the inner (I) and outer (II) leaflets corresponds to the middle of the lipid bilayer. Note that the curve for the narrower tubes is shifted by about 15 Å to the smaller direction.

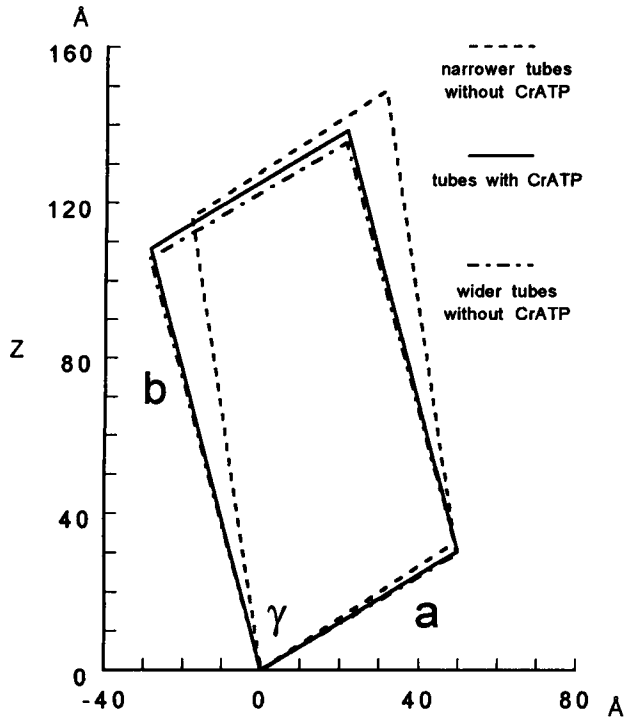


FIGURE 5 Unit cells at the middle of the lipid bilayer for the tubes belonging to the (−25, 7) family after scaling correction. Vertical axis corresponds to the helix axis of tubular crystals (*z*) (Toyoshima and Unwin, 1990). The unit cell parameters are summarized in Table 1.

## Three-dimensional maps of $Ca^{2+}$-ATPase with and without CrATP

Fig. 6 shows the three-dimensional maps of tubular crystals of $Ca^{2+}$-ATPase without CrATP (Fig. 6, *a* and *c*) and those with CrATP (Fig. 6, *b* and *d*) at 14 Å resolution. We show the maps of the tubes of the (−25, 7) family only, because overall structural features of averaged images were virtually identical and a proper *t*-test could be done only with those belonging to this family. The number of images was unequal with the (−26, 7) family for those with and without CrATP. In either map (Fig. 6), a large cytoplasmic domain is linked to the membrane through a stalk region in a similar manner. The positions of the three segments within the membrane are also very similar. A clear difference is found at the groove (*arrowheads* in Fig. 6, *a* and *c*) ascribed previously to the ATP-binding site (Toyoshima et al., 1993a). This groove is filled in the maps of tubes with CrATP (Fig. 6, *b* and *d*).

Fig. 7 shows a fishnet representation of the $Ca^{2+}$-ATPase molecule without CrATP (Fig. 7 *a*) and with CrATP (Fig. 7 *b*). Yellow nets show apparent gains (Fig. 7 *a*) and losses (Fig. 7 *b*) in density in the enzyme with CrATP. The highest peak in Fig. 7 *a* corresponds to twice the standard deviation of the densities in the original three-dimensional maps (corresponding to 4 times the standard deviation in the difference map) and was located in the groove in Fig. 7 *a*. The corresponding peak was also observed in the difference map

**TABLE 2 Image analysis of the tubes belonging to the (−25, 7) family at 14 Å resolution**

| | −CrATP | +CrATP |
|---|---|---|
| Number of tubes averaged | 6 | 7 |
| Number of molecules averaged | 5676 | 6090 |
| Number of layer lines incorporated into the reconstruction | 49 | 50 |
| Twofold phase residuals of the averaged data sets (°)* | 6.2 (narrower tubes)<br>7.5 (wider tubes)# | 4.8 |
| Mean twofold phase residuals of the individual data sets (°) | 19.1 ± 2.0 | 19.6 ± 1.0 |

*Amplitude-weighted phase residuals for twofold symmetry calculated after averaging of weakly and strongly defocused pairs of images, within the first CTF zeros of weakly underfocused images (difference from either 0° or 180°, whichever is closer). The calculation used all of the points with amplitudes higher than 3% of the highest off-equatorial amplitude. The equator was omitted from the calculation.

#Because narrower and wider tubes had different unit cell parameters (Table 1), twofold phase residuals of these two groups were calculated separately.

for the tubes belonging to the (−26, 7) family (data not shown).

To examine the statistical significance of the differences, Student's *t*-test was carried out. Red nets in Fig. 7 enclose the regions where the probability that the differences were real and not due to chance is 99.5% in Fig. 7 *a* and 99.9% in Fig. 7 *b*. At 99.9% confidence level, only a single peak exists in the groove, at the identical position to the highest peak in the difference map (Fig. 7 *a*, *yellow net*). This location is also marked in Fig. 6, *b* and *d* (*white stars*). It is slightly offset from the center of the groove, but not at the outer surface of the enzyme (Fig. 6, *b* and *d*); it is located 10 Å inside the entrance of the groove (Fig. 6, *b* and *d*).

As a control, we compared two groups whose members were randomly selected, ignoring the presence or absence of CrATP. In this control experiment, there were only small gains or losses in density—only 1.33 times the standard deviation at the highest. Furthermore, the significance at this location was less than the 97% confidence level. On the other hand, there were a few points at the 99% confidence level, but the differences themselves were small and were located on the surface of the enzyme; above the 99.5% confidence level none existed (data not shown). Thus, in the control experiment, the difference map and the *t*-map were inconsistent, which is typical of noisy data. In contrast, in the proper difference map, the density gain in the groove (Fig. 7 *a*, *yellow net*) was high and consistent with the *t*-map (Fig. 7 *a*, *red net*). Hence it must represent the real difference caused by the binding of CrATP to $Ca^{2+}$-ATPase.

## DISCUSSION

In this paper we described the differences in the three-dimensional structure of tubular crystals of $Ca^{2+}$-ATPase formed with and without CrATP. With these tubular crystals we determined that the ATPase activity was inhibited, showing that CrATP remained bound, although occluded $Ca^{2+}$ was released (Fig. 2). By cryoelectron microscopy and quantitative image analysis, we found a clear difference at the groove in the cytoplasmic domain (Figs. 6 and 7). This difference was statistically significant at a confidence level higher than 99.9% (Fig. 7 *b*). Except for this difference, the structure of the enzyme with CrATP appeared very similar to that without CrATP (Figs. 6 and 7).

### Position of the ATP-binding site

The ATP-binding site was assigned to the groove in the cytoplasmic domain (Toyoshima et al., 1993a) based on the results by affinity labeling (Yamamoto et al., 1989). The difference map and the *t*-map shown in Fig. 7 indicate that this assignment was correct. In the difference map, the highest peak (4 times the standard deviation of the densities in the difference map) was located in the groove. This difference was confirmed to be statistically significant by *t*-test at a confidence level higher than 99.9% (Fig. 7 *b*, *red net*). The distances between the ATP-binding site and phospholipid/water interface have previously been measured to be 40–60 Å by fluorescence energy transfer (Teruel and Gomez-Fernandez, 1986; Gutierrez-Merino et al., 1987; Bigelow and Inesi, 1991; Baker et al., 1994). In the structure described here, the distance was 43 Å between the point of the most significant difference in the groove (Fig. 6, *b* and *d*, *white stars*; Fig. 7 *b*, *red net*) and the surface of the membrane. This value is consistent with the measurement for Cys344/Cys364 (40 Å), which bracket Asp-351, the residue of phosphorylation (Bigelow and Inesi, 1991).

Similar experiments have been carried out to measure the distances between the ATP-binding site and lanthanide-binding sites (Highsmith and Murphy, 1984; Scott, 1985; Squier et al., 1987). The reported values (16–35 Å) are smaller than those measured from the membrane surface to the ATP-binding site, and lanthanides are thought to bind to the stalk (Squier et al., 1990; Ogurusu et al., 1991; Henao et al., 1992). In particular, Herrmann and Shamoo (1988) measured the distance between bound CrATP and lanthanide ($Eu^{3+}$) to be ~18 Å. This value implies that $Eu^{3+}$ binds to the top of the stalk in our map (Fig. 6).

The whole CrATP molecule remains bound to the enzyme, even after 16 h of incubation (Vilsen and Andersen, 1992), which is long enough for tubular crystal formation. CrATP has a molecular weight of 559 and measures roughly 15 Å in diameter. It is presumably too small to be visualized

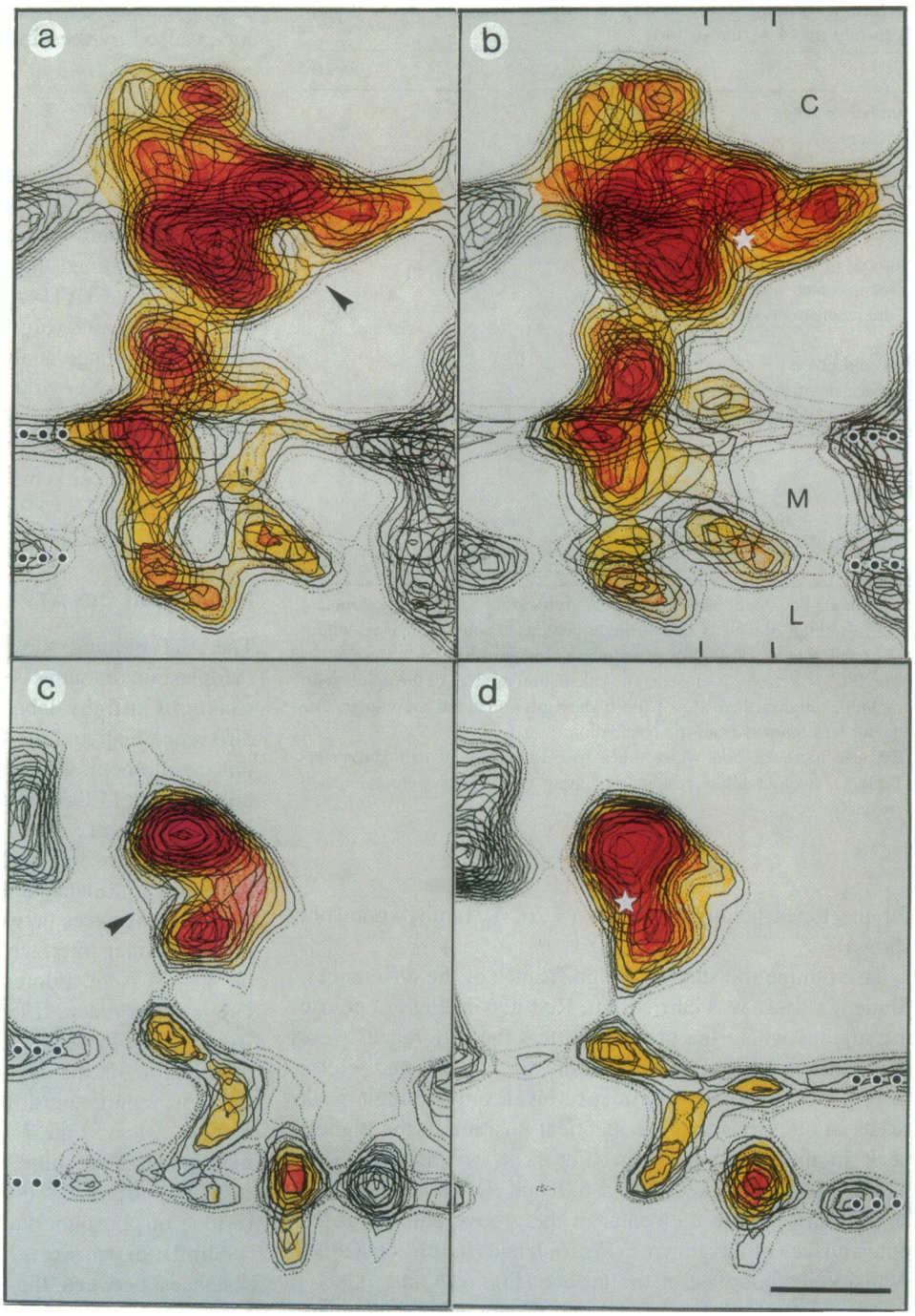


FIGURE 6 Three-dimensional structure of $Ca^{2+}$-ATPase without CrATP (*a,c*) and that with CrATP bound (*b,d*) at 14 Å resolution. (*a,b*) Views perpendicular to the dimer ribbon. C, M, and L in *b* indicate the cytoplasmic, the membrane, and the lumenal regions, respectively. (*c,d*) Stacks of sections (13 Å thick) showing the structure around the groove. The sections are viewed along the dimer ribbon from the left-hand side in *a* and *c* and cover the area specified in *b* by the vertical bars at the top and bottom margins. Note that the groove indicated by the arrowheads in *a* and *c* is filled in *b* and *d*. White stars in *b* and *d* indicate the position of the most significant difference as determined by Student's *t*-test. The lowest solid contours correspond to about 75% of the expected volume. The scale bar represents 25 Å.

at 14 Å resolution as a separate entity when filling the ATP-binding pocket (Fig. 6, *a* and *c*). Nevertheless, because the groove was resolved as a hole of $20 \times 10 \times 7$ Å$^3$ in the enzyme without bound nucleotides, it is likely that the density filling the groove shows up in the difference map. It is also expected that the improvement of resolution will allow us to directly image the CrATP in the groove. Indeed, in our preliminary map at 9 Å resolution, we see a separate density of ~10 Å diameter. On the other hand, we must of course expect structural changes in the protein around the nucleotide-binding site, as has been demonstrated for adenylate kinase (Schulz, 1991). Therefore, we cannot say that the gained densities represent a CrATP molecule. However, because the difference is well localized and no statistically significant density loss is found in the map, it is very likely that the density in the groove really represents CrATP.

## Conformation of $Ca^{2+}$-ATPase with CrATP in the tubular crystals

Although it is well established that CrATP traps two $Ca^{2+}$s and locks the enzyme in the "occluded" state, it is not

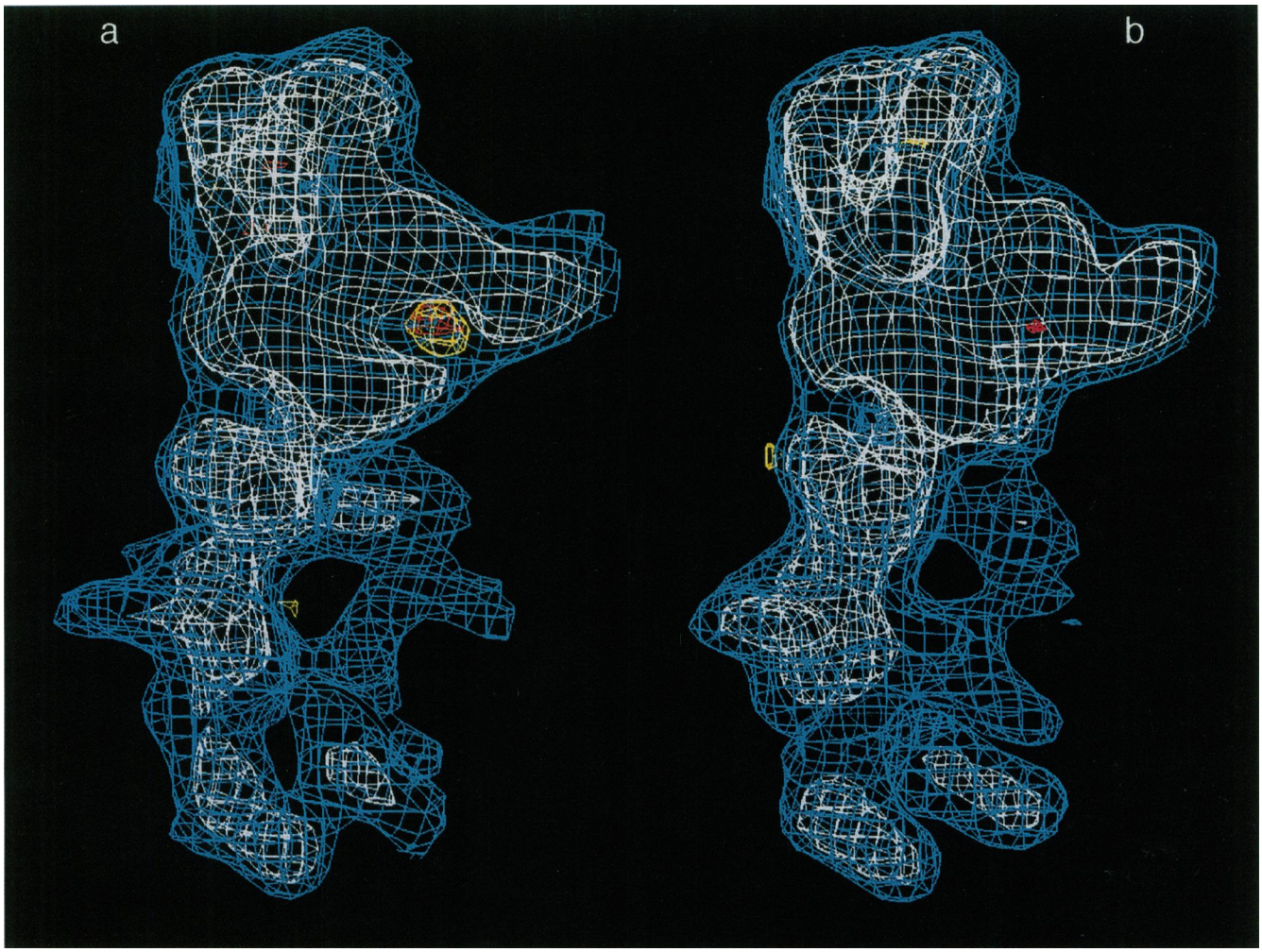


FIGURE 7 Fishnet representation of a part of one $Ca^{2+}$-ATPase molecule viewed from slightly above the membrane. (*a*) The structure without CrATP. (*b*) The structure with CrATP bound. Blue and white nets enclose 75% and 35% of the expected volume, respectively. Yellow nets show gains (*a*) and losses (*b*) in density in the structure with CrATP; the nets enclose the regions where the difference is larger than 1.33 times standard deviation of the densities in the original density map before subtraction. Red nets correspond to the 99.5% (*a*) and 99.9% (*b*) confidence level. Note that the regions of the largest difference and the most significant difference coincide and are located within the groove specified in *a*.

obvious whether the enzyme molecules are in the occluded state in the tubular crystals, because vanadate and EGTA had to be added to induce the crystals. CrATP was still bound in the tubular crystals (Fig. 2, *filled circle after 20 h*; Stokes and Lacapere, 1994; Buhle et al., 1983), but most of the trapped $Ca^{2+}$ was released to make the $Ca^{2+}$-binding site vacant (Fig. 2, *filled box after 20 h*). This result is in apparent conflict with the results of Buhle et al. (1983), but agrees well with Vilsen and Andersen (1992) and Coan et al. (1994). Vilsen and Andersen (1992) measured the amount of bound $^{45}Ca^{2+}$ to be less than 1/10 at 15 h after the addition of EGTA.

An electron paramagnetic resonance (EPR) spectroscopy study gives us some clue. With the iodoacetamide-labeled enzyme, the same EPR spectral changes as those found in the presence of both MgATP and $Ca^{2+}$ were observed in the presence of CrATP alone, irrespective of the presence or the absence of $Ca^{2+}$ (Chen et al., 1991). It indicates that the same structural changes, induced by CrATP in the presence of $Ca^{2+}$, also occur in the ATP-binding site, even in the absence of $Ca^{2+}$. In addition, the enzyme can make a stable complex with CrATP in the absence of $Ca^{2+}$, and the high affinity $Ca^{2+}$-binding sites can be filled afterward (Coan et al., 1994). Hence the enzyme with bound CrATP is thought to remain in the $Ca^{2+}$-occluded state, whereas bound $Ca^{2+}$ has been released (Coan et al., 1994). A proteolysis study also supports this idea (Vilsen and Andersen, 1987).

Nevertheless, the matter seems more complicated because of the presence of vanadate used to induce tubular crystals. Although the vanadate solution that we used consists mostly of decavanadate, it contains monomers and other oligomeric species of vanadates (Csermely et al., 1985; Aureliano and Madeira, 1994). It alters the ATPase activity, although the mobility of the membrane domain is reported to be unchanged (Lewis and Thomas, 1986). Therefore, the presence of vanadate is likely to alter the

structure of the cytoplasmic domains. In fact, the trypsin digestion pattern of the tubes with bound CrATP in the presence of vanadate was different, depending on the presence or the absence of $Ca^{2+}$, and was identical to that of the enzyme without CrATP (unpublished observation). Further experiments will be needed to characterize the state of the enzyme in these tubular crystals.

### Structural differences in other sites

There are a few other sites where the differences are statistically significance at a confidence level higher than 99.5%. At the top of the cytoplasmic domain (Fig. 7 *a*, *red nets*), small gains or losses in density are found, corresponding to 1.2 times the standard deviation of the densities in the original map. From its position next to the groove assigned as the ATP-binding pocket, this region is a good candidate for the $\beta$-strand domain, which has an essential role in phosphoenzyme turnover (Andersen et al., 1989; Clarke et al., 1990b).

We had expected to find structural changes in either the stalk or the transmembrane domain, but found no significant differences in these regions (Fig. 7). This fact may imply that the CrATP-bound enzyme is not truly in the occluded state in the tubular crystals, but in a special conformation forced by vanadate. That is, the binding signal of ATP may have been blocked and could not be conducted to the stalk or to the membrane domain. Of course, we cannot exclude the possibility that structural changes in these domains are too small to be resolved at 14 Å resolution, and improved resolution is needed for the visualization. In the case of the acetylcholine receptor, 9 Å resolution was needed to visualize the rearrangement caused by the binding of acetylcholine, of $\alpha$-helices surrounding the pore (Unwin, 1995). We are hopeful that we will be able to visualize such conformational changes in the near future.

## CONCLUSIONS

On the basis of the three-dimensional image analysis, we conclude that the ATP-binding site is located in the groove of the cytoplasmic domain. This is the first functional site located directly on the three-dimensional structure and will provide the origin for mapping of other functional sites.

We gratefully thank Prof. T. Tsukihara of the Institute for Protein Research, Osaka University, for a set of real-space-fitting programs and K. Tani for implementing these programs on our computers.

This work was supported in part by Grants-in-Aid for Scientific Research from the Ministry of Education, Science, Sports and Culture of Japan.

## REFERENCES

Andersen, J. P., B. Vilsen, E. Leberer, and D. H. MacLennan. 1989. Functional consequences of mutations in the beta-strand sector of the $Ca^{2+}$-ATPase of sarcoplasmic reticulum. *J. Biol. Chem.* 264: 21018–21023.

Aureliano, M., and V. M. Madeira. 1994. Interactions of vanadate oligomers with sarcoplasmic reticulum $Ca^{2+}$-ATPase. *Biochim. Biophys. Acta.* 1221:259–271.

Baker, K. J., J. M. East, and A. G. Lee. 1994. Localization of the hinge region of the $Ca^{2+}$-ATPase of sarcoplasmic reticulum using resonance energy transfer. *Biochim. Biophys. Acta.* 1192:53–60.

Bigelow, D. J., and G. Inesi. 1991. Frequency-domain fluorescence spectroscopy resolves the location of maleimide-directed spectroscopic probes within the tertiary structure of the Ca-ATPase of sarcoplasmic reticulum. *Biochemistry.* 30:2113–2125.

Bigelow, D. J., and G. Inesi. 1992. Contributions of chemical derivatization and spectroscopic studies to the characterization of the $Ca^{2+}$ transport ATPase of sarcoplasmic reticulum. *Biochim. Biophys. Acta.* 1113: 323–338.

Brandl, C. J., N. M. Green, B. Korczak, and D. H. MacLennan. 1986. Two $Ca^{2+}$-ATPase genes: homologies and mechanistic implication of deduced amino acid sequences. *Cell.* 44:597–607.

Buhle, E. L., Jr., B. E. Knox, E. Serpersu, and U. Aebi. 1983. The structure of the $Ca^{2+}$-ATPase as revealed by electron microscopy and image processing of ordered arrays. *J. Ultrastruct. Res.* 85:186–203.

Caspar, D. L. D., C. Cohen, and W. Longley. 1969. Tropomyosin: crystal structure, polymorphism and molecular interactions. *J. Mol. Biol.* 41: 87–107.

Chen, Z. D., C. Coan, L. Fielding, and G. Cassafer. 1991. Interaction of CrATP with the phosphorylation site of the sarcoplasmic reticulum ATPase. *J. Biol. Chem.* 266:12386–12394.

Chen, L., C. Sumbilla, D. Lewis, L. Zhong, C. Strock, M. E. Kirtley, and G. Inesi. 1996. Short and long range functions of amino acids in the transmembrane region of the sarcoplasmic reticulum ATPase. *J. Biol. Chem.* 271:10745–10752.

Clarke, D. M., T. W. Loo, G. Inesi, and D. H. MacLennan. 1989. Location of high affinity $Ca^{2+}$-binding sites within the predicted transmembrane domain of the sarcoplasmic reticulum $Ca^{2+}$-ATPase. *Nature.* 339: 476–478.

Clarke, D. M., T. W. Loo, and D. H. MacLennan. 1990a. Functional consequences of alterations to amino acids located in the nucleotide binding domain of the $Ca^{2+}$-ATPase of sarcoplasmic reticulum. *J. Biol. Chem.* 265:22223–22227.

Clarke, D. M., T. W. Loo, and D. H. MacLennan. 1990b. Functional consequences of mutations of conserved amino acids in the $\beta$-strand domain of the $Ca^{2+}$-ATPase of sarcoplasmic reticulum. *J. Biol. Chem.* 265:14088–14092.

Cleland, W. W. 1982. Preparation of chromium(III) and cobalt(III) nucleotides as chirality and inhibitors. *Methods Enzymol.* 87:159–179.

Coan, C., J. Y. Ji, and J. A. Amaral. 1994. $Ca^{2+}$ binding to occluded sites in the CrATP-ATPase complex of sarcoplasmic reticulum: evidence for two independent high-affinity sites. *Biochemistry.* 33:3722–3731.

Csermely, P., A. Martonosi, G. C. Levy, and A. J. Ejchart. 1985. $^{51}$V-n.m.r. analysis of the binding of vanadium(V) oligoanions to sarcoplasmic reticulum. *Biochem. J.* 230:807–815.

Green, N. M., and D. L. Stokes. 1992. Structural modelling of P-type ion pumps. *Acta Physiol. Scand. Suppl.* 607:59–68.

Gutierrez-Merino, C., F. Munkonge, A. M. Mata, J. M. East, B. L. Levinson, R. M. Napier, and A. G. Lee. 1987. The position of the ATP binding site on the ($Ca^{2+}$ + $Mg^{2+}$)-ATPase. *Biochim. Biophys. Acta.* 897:207–216.

Henao, F., S. Orlowski, Z. Merah, and P. Champeil. 1992. The metal sites on sarcoplasmic reticulum membranes that bind lanthanide ions with the highest affinity are not the ATPase $Ca^{2+}$ transport sites. *J. Biol. Chem.* 267:10302–10312.

Herrmann, T. R., and A. E. Shamoo. 1988. Estimation of inter-binding-site distances in sarcoplasmic reticulum ($Ca^{2+}$ + $Mg^{2+}$)-ATPase under occluded and non-occluded conditions. *Mol. Cell Biochem.* 82:55–58.

Highsmith, S., and A. J. Murphy. 1984. $Nd^{3+}$ and $Co^{2+}$ binding to sarcoplasmic reticulum CaATPase. An estimation of the distance from the ATP binding site to the high-affinity calcium binding sites. *J. Biol. Chem.* 259:14651–14656.

Lewis, S. M., and D. D. Thomas. 1986. Effects of vanadate on the rotational dynamics of spin-labeled calcium adenosinetriphosphatase in sarcoplasmic reticulum membranes. *Biochemistry.* 25:4615–4621.

MacLennan, D. H., C. J. Brandl, B. Korczak, and N. M. Green. 1985. Amino-acid sequence of a $Ca^{2+}$ + $Mg^{2+}$-dependent ATPase from rabbit muscle sarcoplasmic reticulum, deduced from its complementary DNA sequence. *Nature.* 316:696–700.

Mariano, D. D., and W. W. Cleland. 1980. Preparation and properties of chromium(III) adenosine 5′-triphosphate, chromium(III) adnosine 5′-diphosphate, and related chromium(III) complexes. *Biochemistry.* 19: 1496–1505.

Maruyama, K., D. M. Clarke, J. Fujii, G. Inesi, T. W. Loo, and D. H. MacLennan. 1989. Functional consequences of alterations to amino acids located in the catalytic center (isoleucine 348 to threonine 357) and nucleotide-binding domain of the $Ca^{2+}$-ATPase of sarcoplasmic reticulum. *J. Biol. Chem.* 264:13038–13042.

Meissner, G., G. E. Conner, and S. Fleischer. 1973. Isolation of sarcoplasmic reticulum by zonal centrifugation and purification of $Ca^{2+}$-pump and $Ca^{2+}$-binding proteins. *Biochim. Biophys. Acta.* 298:246–269.

Milligan, R. A., and P. F. Flicker. 1987. Structural relationships of actin, myosin and tropomyosin revealed by cryo-electron microscopy. *J. Cell Biol.* 105:29–39.

Møller, J. V., B. Juul, and M. le Maire. 1996. Structural organization, ion transport, and energy transduction of P-type ATPases. *Biochim. Biophys. Acta.* 1286:1–51.

Ogurusu, T., S. Wakabayashi, and M. Shigekawa. 1991. Functional characterization of lanthanide binding sites in the sarcoplasmic reticulum $Ca^{2+}$-ATPase: do lanthanide ions bind to the calcium transport site? *Biochemistry.* 30:9966–9973.

Schulz, G. E. 1991. Domain motions in proteins. *Curr. Opin. Struct. Biol.* 1:883–888

Scott, T. L. 1985. Distances between the functional sites of the ($Ca^{2+}$ + $Mg^{2+}$)-ATPase of sarcoplasmic reticulum. *J. Biol. Chem.* 260: 14421–14423.

Serpersu, E. H., U. Kirch, and W. Schoner. 1982. Demonstration of a stable occuluded form of $Ca^{2+}$ by the use of the chromium complex of ATP in the $Ca^{2+}$-ATPase of sarcoplasmic reticulum. *Eur. J. Biochem.* 122: 347–354.

Smith, P. K., R. I. Krohn, G. T. Hermanson, A. K. Mallia, F. H. Gartner, M. D. Provenzano, E. K. Fujimoto, N. M. Goeke, B. J. Olson, and D. C. Klenk. 1985. Measurement of protein using bicinchoninic acid. *Anal. Biochem.* 150:76–85.

Squier, T. C., D. J. Bigelow, F. J. Fernandez-Belda, L. de Meis, and G. Inesi. 1990. Calcium and lanthanide binding in the sarcoplasmic reticulum ATPase. *J. Biol. Chem.* 265:13713–13720.

Squier, T. C., D. J. Bigelow, J. Garcia de Ancos, and G. Inesi. 1987. Localization of site-specific probes on the Ca-ATPase of sarcoplasmic reticulum using fluorescence energy transfer. *J. Biol. Chem.* 262: 4748–4754.

Stokes, D. L., and J. J. Lacapere. 1994. Conformation of $Ca^{2+}$-ATPase in two crystal forms. Effects of $Ca^{2+}$, thapsigargin, adenosine 5′-($\beta$,$\gamma$-methylene)triphosphate), and chromium(III)-ATP on crystallization. *J. Biol. Chem.* 269:11606–11613.

Tani, K., H. Sasabe, and C. Toyoshima. 1996. A set of programs for determining defocus and astigmatism in electron images. *Ultramicroscopy.* 65:31–44.

Taylor, W. R., and N. M. Green. 1989. The predicted secondary structures of the nucleotide-binding sites of six cation-transporting ATPases lead to a probable tertiary fold. *Eur. J. Biochem.* 179:241–248.

Teruel, J. A., and J. C. Gomez-Fernandez. 1986. Distances between the functional sites of sarcoplasmic reticulum ($Ca^{2+}$ + $Mg^{2+}$)-ATPase and the lipid/water interface. *Biochim. Biophys. Acta.* 863:178–184.

Thorley-Lawson, D. A., and N. M. Green. 1973. Studies on the location and orientation of proteins in the sarcoplasmic reticulum. *Eur. J. Biochem.* 40:403–413.

Toyoshima, C., H. Sasabe, and D. L. Stokes. 1993a. Three-dimensional cryo-electron microscopy of the calcium ion pump in the sarcoplasmic reticulum membrane. *Nature.* 362:469–471.

Toyoshima, C., and N. Unwin. 1988. Ion channel of acetylcholine receptor reconstructed from images of postsynaptic membranes. *Nature.* 336: 247–250.

Toyoshima, C., and N. Unwin. 1990. Three-dimensional structure of the acetylcholine receptor by cryoelectron microscopy and helical image reconstruction. *J. Cell Biol.* 111:2623–2635.

Toyoshima, C., K. Yonekura, and H. Sasabe. 1993b. Contrast transfer for frozen-hydrated specimens. II. Amplitude contrast at very low frequencies. *Ultramicroscopy.* 48:165–176.

Unwin, N. 1995. Acetylcholine receptor channel imaged in the open state. *Nature.* 373:37–43.

Varga, S., P. Csermely, and A. Martonosi. 1985. The binding of vanadium (V) oligoanions to sarcoplasmic reticulum. *Eur. J. Biochem.* 148: 119–126.

Vilsen, B., and J. P. Andersen. 1987. Characterization of CrATP-induced calcium occlusion in membrane-bound and soluble monomeric sarcoplasmic reticulum $Ca^{2+}$-ATPase. *Biochim. Biophys. Acta.* 898:313–322.

Vilsen, B., and J. P. Andersen. 1992. Interdependence of $Ca^{2+}$ occlusion sites in the unphosphorylated sarcoplasmic reticulum $Ca^{2+}$-ATPase complex with CrATP. *J. Biol. Chem.* 267:3539–3550.

Vilsen, B., J. P. Andersen, and D. H. MacLennan. 1991. Functional consequences of alterations to amino acids located in the hinge domain of the $Ca^{2+}$-ATPase of sarcoplasmic reticulum. *J. Biol. Chem.* 266: 16157–16164.

Warren, G. B., P. A. Toon, N. J. Birdsall, A. G. Lee, and J. C. Metcalfe. 1974. Reconstitution of a calcium pump using defined membrane components. *Proc. Natl. Acad. Sci. USA.* 71:622–626.

Yamamoto, H., Y. Imamura, M. Tagaya, T. Fukui, and M. Kawakita. 1989. $Ca^{2+}$-dependent conformational change of the ATP-binding site of $Ca^{2+}$-transporting ATPase of sarcoplasmic reticulum as revealed by an alteration of the target-site specificity of adenosine triphosphopyridoxal. *J. Biochem.* 106:1121–1125.